PAPER • **OPEN ACCESS**

Mode properties of telecom wavelength InP-based high-(Q/*V*) L4/3 photonic crystal cavities

To cite this article: L Rickert *et al* 2020 *Nanotechnology* **31** 315703

OPEN ACCESS
IOP Publishing
Nanotechnology

Nanotechnology **31** (2020) 315703 (5pp)
https://doi.org/10.1088/1361-6528/ab8a8c

Mode properties of telecom wavelength InP-based high-(Q/*V*) L4/3 photonic crystal cavities

L Rickert, B Fritsch, A Kors, J P Reithmaier and M Benyoucef

Institute of Nanostructure Technologies and Analytics (INA), Center of Interdisciplinary Nanostructure Science and Technology (CINSaT), University of Kassel, Heinrich-Plett-Straße 40, Kassel 34132, Germany

E-mail: m.benyoucef@physik.uni-kassel.de

Received 10 December 2019, revised 28 February 2020
Accepted for publication 17 April 2020
Published 13 May 2020

Abstract

We present finite-difference time domain simulations and optical characterizations via micro-photoluminescence measurements of InP-based L4/3 photonic crystal cavities with embedded quantum dots (QDs) and designed for the M1 ground mode to be emitting at telecom C-band wavelengths. The simulated M1 Q-factor values exceed 10^6, while the M1 mode volume is found to be $0.33 \times (\lambda/n)^3$, which is less than half the value of the M1 mode volume of a comparable L3 cavity. Low-temperature micro-photoluminescence measurements revealed experimental M1 Q-factor values on the order of 10^4 with emission wavelengths around 1.55 μm. Weak coupling behavior of the QD exciton line and the M1 ground mode was achieved via temperature-tuning experiments.

Keywords: photonic crystal, telecom wavelength, quantum dots, spectroscopy

(Some figures may appear in colour only in the online journal)

1. Introduction

Strong-coupling phenomena in an atom-like emitter–cavity system hold huge potential for quantum information processing applications, such as being fundamental building blocks for quantum-phase gates [1] and quantum computing schemes [2]. Semiconductor quantum dots (QDs) embedded in photonic crystal (PhC) cavities are promising candidates to achieve strong-coupling phenomena in a solid-state platform, and offer the potential of scalable quantum systems. Strong coupling in GaAs-based PhC cavities with embedded InAs QDs was already observed in the mid 2000s [3, 4], with emission wavelengths below 1000 nm [5–9], which is not compatible with fiber-based quantum communication.

InP-based QDs, on the other hand, offer the possibility to achieve high-quality (single) QD emission around 1.5 μm [10] with vanishing fine-structure splitting [11]. Fabrication and optical investigation of InP-based L3 PhC cavities showing a weak-coupling regime have recently been reported [12–14]. Several factors can influence the coupling behavior of a cavity– QD system, including spectral and spatial matching of the mode and QD, as well as the optical qualities of the cavity. Regarding the latter, the fraction of quality factor to mode volume Q/V needs to be as high as possible to achieve strong coupling [15]. Therefore, PhC cavities with large Q-factors and small mode volume are desired. The L3 PhC cavity is a commonly used design, which is formed by three missing air-holes in a hexagonal air-hole lattice in a free-standing semiconductor membrane. Q-factor values of about a few 10^4 to 10^5 for passive silicon-based L3 cavities have been reported [16, 17], which could be increased to more than 10^6 by further design optimization (e.g. hole shift) [18–22].

The M1 ground mode volume for L3-cavities is on the order of $0.8\ (\lambda/n)^3$ [3, 17, 23], which is sufficient to achieve strong coupling in GaAs-based PhCs with embedded QDs for

Q-factors of 13 300 [4], or even as low as 9200 if the spatial overlap between the QD and PhC is ensured [6]. The lower experimentally observed Q-factors of GaAs-based PhCs containing QDs are likely caused by additional absorption compared to passive Si-based PhCs and a less developed fabrication process. This might affect the InP material system even more, since fabrication is even less established than for the case of GaAs PhCs, which likely explains the currently reported highest Q-factors for the M1 mode being limited to below 8600 [12] and the fact that no observation of strong coupling has yet been reported.

To achieve the strong-coupling regime in InP-based PhC cavities, a decrease in mode volume is desirable in order to increase the Q/V value. This requires a change in the cavity design to reduce the mode volume and an improvement in the fabrication process to increase the experimental Q-factor. Based on a theoretical work, Minkov *et al* have proposed an alternative PhC cavity design, for which they found simulated ground mode Q-factors of tenths of millions and reduction of the mode volume to about $V \sim 0.32 \times (\lambda/n)^3$ [24]. This design is called the L4/3 PhC cavity, and is also based on a hexagonal air-hole lattice but, instead of forming the cavity by removing three holes as in the L3 cavity case, four holes are introduced as shown in figure 1(a). The reduced amount of dielectric material causes a reduction in mode volume of more than a factor of two compared to the L3 design. The L4/3 PhC is regarded as superior to the L3 PhC design for achieving the strong-coupling regime due to the increased Q/V ratio [24]. Taking into account the reported experimental Q-factors for InP-based L3 PhC cavities, a strong coupling could be feasible for the L4/3 PhC design due to decreased mode volume [12]. It should be noted that, although there are other cavity designs with even higher reported Q-factors, and comparable Q/V to the L4/3 design for passive silicon devices [25], these designs do not achieve as small mode volumes as the L4/3 cavity. The high Q/V in this case is achieved by the Q-factor, which is more susceptible to fabrication than the mode volume.

In this work, we report on simulation and fabrication of InP-based L4/3 PhC cavities for telecom C-band emission around 1.55 μm. The PhC cavities with embedded InAs QDs emitting are successfully fabricated using electron beam lithography and different etching steps. The optical properties of the fabricated cavities are investigated using polarization-dependent micro-photoluminescence (μ-PL) spectroscopy. Low-temperature PL measurements show sharp cavity modes with Q-factors exceeding 10 000. Due to the random distribution of the embedded dots in the cavities, temperature-tuning experiments with a suitable QD could only be carried out for an L4/3 cavity with a Q-factor of 5600, showing weak coupling of a QD emission line with the cavity mode.

2. Methods

Three-dimensional finite-difference time domain (3D-FDTD) simulations [26] were carried out to simulate the properties of L4/3 PhC cavities [24]. The simulation area consisted of a slab with thickness t and a constant refractive index

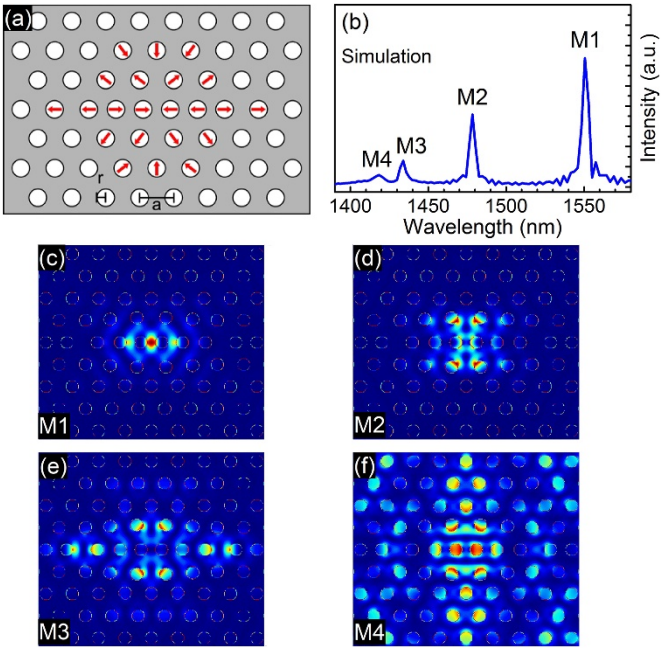

Figure 1. (a) L4/3 cavity layout with inner-hole shifts of 0.005a to 0.2a. (b) Simulated L4/3 cavity spectrum exhibiting four modes labeled M1 to M4. (c)–(f) $|E|^2$ near-field distribution of the M1, M2, M3 and M4 modes shown in the spectrum (b).

($n_{\mathrm{InP,\ 300\ K}} = 3.1467$) with a hole radius r and a lattice-period a. TE-dipole sources were used for excitation of the cavity modes. Near-field data were recorded at the center of the slab plane ($z = 0$). The investigated samples consisted of InAs QDs of medium density embedded in an InP-matrix grown on top of a sacrificial layer by solid-source molecular beam epitaxy. The ensemble QD emission covered a relatively wide range of wavelengths starting from ~1200 nm to about 1650 nm with a maximum PL intensity centred arround 1550 nm at cryogenic temperature. A similar fabrication process as in [12] was used to fabricate the PhC cavities. For μ-PL measurements, the samples were placed inside a helium-flow cryostat. A continuous-wave laser ($\lambda = 532$ nm), focused by an objective with numerical aperture of 0.7 to a spot size of ~1 μm was used for optical excitation. The emitted light was collected through the same objective and spectrally filtered by a 0.75 m focal length spectrometer, equipped with a liquid nitrogen-cooled InGaAs detector.

3. Results

Figure 1(a) shows the layout of the L4/3 cavity with inner-hole shifts [24], proposed for optimization of the M1 mode Q-factor. Figure 1(b) displays the cavity mode spectrum obtained from the FDTD simulation. To simulate the emission wavelength and mode volume a simulation grid resolution of $0.1a$ was used. In the FDTD simulations, the following values were used: $a = 420$ nm, $r = 110$ nm and $t = 310$ nm with hole shifts of $0.005a$ to $0.2a$ Four distinct peaks are identified, corresponding to four cavity modes labeled as M1 to M4, where near-fields are displayed in figure 1(c)–(f). The simulated M1

ground mode emission appears at around 1.55 μm with mode volume $V_{M1} \sim 0.33 \times (\lambda/n)^3$. A simulated Q-factor value of $Q_{M1} \sim 3.8 \times 10^6$ is obtained, which is an order of magnitude smaller than those reported in [24] for the same applied hole shift design in Si. This is expected considering the low grid resolution used of $0.1a$. We checked the influence of the resolution on the obtained Q-factor for the Si-based L4/3 cavity in [24] with our simulation. Using a two-fold finer grid size than for the InP-based simulation (i.e. $0.05a$) results in $Q_{M1,Si} \sim 7.4 \times 10^6$, which is on the same order as for the case of the InP-based PhC. Note that the slight changes in r and t for the InP-based PhC cavity could additionally lower the Q-values. These results show that the InP-based L4/3 cavity can exhibit high theoretical Q-factors of at least 10^6 while being able to achieve 2–3 times smaller mode volumes for the M1 ground mode compared to an InP-based L3 cavity, and thus can provide a better Q/V ratio.

Though the work in [24] was focused on the properties of the M1 ground mode, in the present work we show that L4/3 PhC cavities are also able to support higher modes, as can be seen in figure 1(b). The M2 mode has the highest simulated $Q_{M2} \sim 7300$ among the observed modes but larger mode volume compared to the M1 mode, as can be seen in the near-field profile of figure 1(d). It should be noted that the additional modes only appear in the simulated spectra if the hole shifts are applied to the cavity. The L4/3 cavity without hole-shift optimization only supports the M1 ground mode.

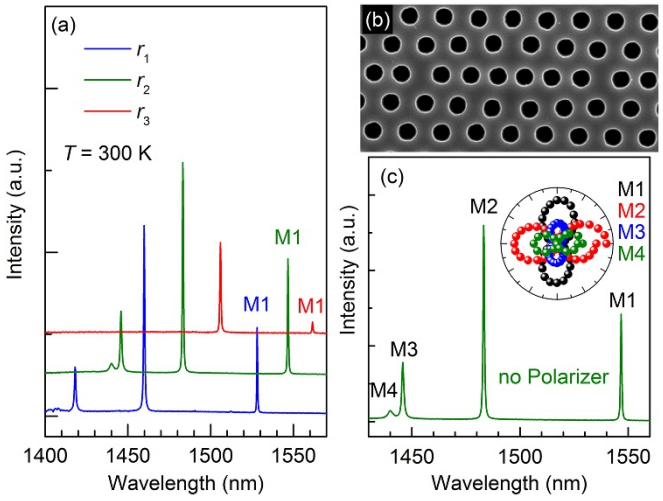

Figure 2. (a) Room temperature μ-PL spectra of PhC L4/3 cavities with constant period a and thickness t and varying hole radius $r_1 \sim 110$ nm $> r_2 \sim 100$ nm $> r_3 \sim 90$ nm taken at $\sim$100 μW excitation power. (b) Scanning electron microscope image of the InP-based L4/3 cavity. (c) Unpolarized μ-PL spectrum of the cavity with radius r_2. The inset shows the polarization dependence of the four identified cavity modes.

Figure 2 shows room temperature μ-PL data for the fabricated InP-based based L4/3 cavities with varying hole size, as well as polarization-dependent measurements. Figure 2(a) displays the μ-PL spectra taken at room temperature for cavities with identical period length $a \sim 420$ nm and membrane thickness $t \sim 310$ nm, but with different hole radii $r_1 \sim 110$ nm $> r_2 \sim 100$ nm $> r_3 \sim 90$ nm. As can be seen, the sharp peak at lowest energy, which is attributed to the respective cavity ground mode M1, fits the expected wavelength of around 1.55 μm well for the $\sim$ 100 nm radius. In figure 2(b), a scanning electron microscope image of the PhC cavity is presented, showing clearly the applied shifts.

To assign the different peaks in the PL spectra, polarization-dependent measurements were performed as shown in figure 2(c) for the cavity with radius r_2. The measured four cavity modes M1 to M4 can be identified and are assigned in the unpolarized spectrum in figure 2(c). M1 and M4 show linearly vertical polarized emission (90°) and M2 and M4 show linearly horizontal polarized emission (0°).

Furthermore, M3 and M4 are clearly visible in the experimental spectra for the cavity with hole radius r_2, whereas the M4 mode is missing for the cavity with hole radius r_1 and very weak for the r_3 cavity, indicating that they are sensitive to the fabrication process.

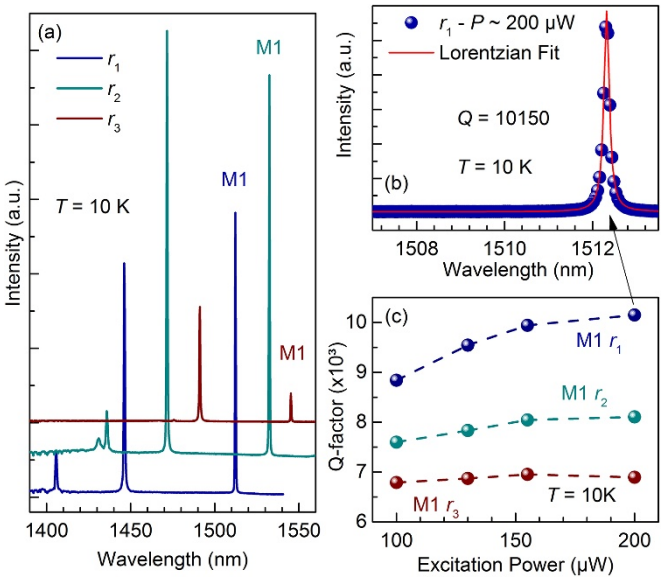

Figure 3. (a) Low-temperature ($T = 10$ K) PL spectra taken at $\sim$100 μW excitation power for the same cavities as in figure 2. (b) High-resolution PL spectrum taken at 10 K and 200 μW excitation power for the cavity with hole radius r_1. The M1 Q-factor exceeds 10 000. (c) M1 Q-factor of the cavities in (a) versus the excitation power.

Figure 3(a) illustrates low-temperature PL spectra of the fabricated PhC cavities taken at high excitation power. By appropriate choice of the hole radius (in this case r_3) M1 emission could be shifted to a telecom C-band wavelength of 1.55 μm. A high-resolution PL spectrum of the M1 mode from the cavity with radius r_1 is shown in figure 3(b) where a Q-factor exceeding 10 000 is measured. Figure 3(c) shows the measured M1 Q-factors of the cavities with varying excitation powers for the three different radii. The Q-factor values

increase with increasing excitation power; this is due to the saturation of QD transitions [27]. Additionally, M2 Q-factors of ∼2900 and ∼3400 were measured for the cavities with radii r_1 and r_2 in agreement with the simulations. For comparison, the experimental Q-factor values of the M2 and M3 modes in an L3 cavity are around 1000 and 400, respectively [13, 23]. Note that the PL spectrum for the cavity with r_3 was obtained using a different fabrication process of the same wafer from that for the cavities with r_1 and r_2. The differences in Q-factor for cavities with these three radii could also be related to the fabrication process.

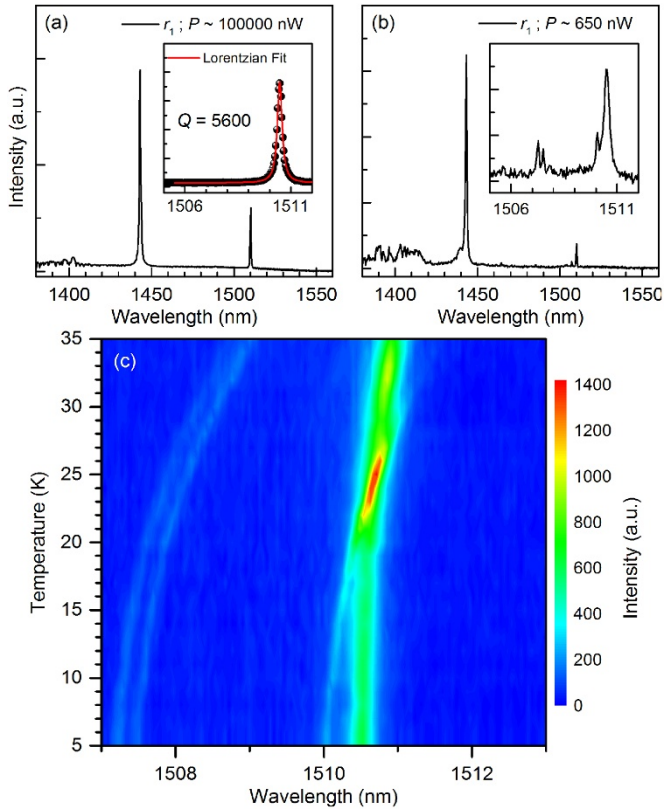

Figure 4. (a) Low-temperature μ-PL spectrum taken at P ∼100 μW excitation power for an L4/3 cavity with hole radius r_1. (b) μ-PL spectrum ($T = 10$ K) of the cavity taken at $P \sim 650$ nW excitation power. (c) Temperature-dependent measurements of the excitonic line and M1 mode.

Due to the lack of QDs spectrally near the high Q M1 modes of the cavities in figure 3(a), no temperature-tuning experiments could be carried out for these cavities. An additional low-temperature μ-PL spectrum of a cavity with radius r_1 taken ∼100 μW excitation power is shown in figure 4(a). The measured Q-factor of the M1 mode is about 5600. Reducing the excitation laser power to $P \sim 650$ nW, a sharp emission line near the M1 mode is visible. This line originates from a single QD. The emission of this excitonic line is spectrally very close to the M1 mode and has lower intensity, therefore using power-dependent measurements did not allow us to identify the nature of this excitonic line. Using temperature-dependent measurements, the excitonic line is tuned to the M1 mode, which exhibits an increase in intensity when in resonance with the M1 mode at 24 K, which shows evidence of a weak coupling behavior. The peak intensity of the QD emission line at $T = 5$ K is enhanced by a factor of 6 in the resonance case with M1 at 24 K. This low enhancement is most likely caused by an insufficient spatial overlap of the QD and cavity mode.

4. Conclusion

InP-based L4/3 cavities with high (Q/V) M1 ground mode emitting at 1.55 μm are simulated, fabricated and experimentally investigated by μ-PL spectroscopy. The measured Q-factors of cavities with embedded QDs are found to exceed 10^4. Furthermore, several higher-energy modes are observed in agreement with the FDTD simulations and identified by polarization-dependent measurements. A weak coupling behavior is observed using temperature tuning of the excitonic line to the M1 cavity mode, evidenced by enhancement emission when the excitonic line is in resonance with the cavity mode. These results are encouraging, even though no strong coupling is obtained, that with a reduced cavity mode volume and reasonably high Q-factor, with additional improvement in the fabrication process, strong coupling could be achieved. Further investigations to prove this have to overcome the challenges of spatial and spectral matching of the QD and the cavity mode, e.g. by employing deterministic techniques.

Acknowledgments

We acknowledge K Fuchs, A Vereijken and D Albert for technical support. This work was financially supported by the German Federal Ministry of Education and Research (BMBF) Project (Q.Link.X).

ORCID iD

M Benyoucef https://orcid.org/0000-0002-4756-3818

References

[1] Rauschenbeutel A, Nogues G, Osnaghi S, Bertet P, Brune M, Raimond J M and Haroche S 1999 *Phys. Rev. Lett.* **83** 5166–9
[2] Imamoğlu A, Awschalom D D, Burkard G, DiVincenzo D P, Loss D, Sherwin M and Small A 1999 *Phys. Rev. Lett.* **83** 4204–7
[3] Hennessy K, Badolato A, Winger M, Gerace D, Atatüre M, Gulde S, Fält S, Hu E L and Imamoğlu A 2007 *Nature* **445** 896–9
[4] Yoshie T, Scherer A, Hendrickson J, Khitrova G, Gibbs H M, Rupper G, Ell C, Shchekin O B and Deppe D G 2004 *Nature* **432** 200–3
[5] Ota Y, Ohta R, Kumagai N, Iwamoto S and Arakawa Y 2015 *Phys. Rev. Lett.* **114** 143603
[6] Thon S M, Rakher M T, Kim H, Gudat J, Irvine W T M, Petroff P M and Bouwmeester D 2009 *Appl. Phys. Lett.* **94** 111115
[7] Luxmoore I J *et al* 2013 *Sci. Rep.* **3** 1239

[8] Laucht A, Hauke N, Villas-Bôas J M, Hofbauer F, Böhm G, Kaniber M and Finley J J 2009 *Phys. Rev. Lett.* **103** 87405
[9] Englund D, Majumdar A, Faraon A, Toishi M, Stoltz N, Petroff P and Vucković J 2010 *Phys. Rev. Lett.* **104** 73904
[10] Benyoucef M, Yacob M, Reithmaier J P, Kettler J and Michler P 2013 *Appl. Phys. Lett.* **103** 162101
[11] Kors A, Reithmaier J P and Benyoucef M 2018 *Appl. Phys. Lett.* **112** 172102
[12] Kors A, Fuchs K, Yacob M, Reithmaier J P and Benyoucef M 2017 *Appl. Phys. Lett.* **110** 31101
[13] Kim J-H, Cai T, Richardson C J K, Leavitt R P and Waks E 2016 *Optica* **3** 577
[14] Birowosuto M D, Sumikura H, Matsuo S, Taniyama H, van Veldhoven P J, Nötzel R and Notomi M 2012 *Sci. Rep.* **2** 321
[15] Reithmaier J P 2008 *Semicond. Sci. Technol.* **23** 123001
[16] Akahane Y, Asano T, Song B-S and Noda S 2005 *Opt. Exp.* **13** 1202
[17] Akahane Y, Asano T, Song B-S and Noda S 2003 *Nature* **425** 944–7
[18] Minkov M and Savona V 2014 *Sci. Rep.* **4** 5124
[19] Lai Y, Pirotta S, Urbinati G, Gerace D, Minkov M, Savona V, Badolato A and Galli M 2014 *Appl. Phys. Lett.* **104** 241101
[20] Kuramochi E, Nozaki K, Shinya A, Takeda K, Tomonari S, Matsuo S, Taniyama H, Sumikura H and Notomi M 2014 *Nat. Photonics* **8** 474
[21] Maeno K, Takahashi Y, Nakamura T, Asano T and Noda S 2017 *Opt. Exp.* **25** 367–76
[22] Nakamura T, Takahashi Y, Tanaka Y, Asano T and Noda S 2016 *Opt. Exp.* **24** 9541–9
[23] Chalcraft A R A and Lam S *et al* 2007 *Appl. Phys. Lett.* **90** 241117
[24] Minkov M, Savona V and Gerace D 2017 *Appl. Phys. Lett.* **111** 131104
[25] Kuramochi E, Notomi M, Mitsugi S, Shinya A, Tanabe T and Watanabe S 2006 *Appl. Phys. Lett.* **88** 041112
[26] Lumerical Inc 2018 FDTD Solutions: 3D/2D Maxwell's. solver for nanophotonic devices (https://www.lumerical.com/tcad-products/fdtd/)
[27] Gayral B and Gérard J M 2008 *Phys. Rev.* B **78** 681